Full-band-structure calculation of first-, second-, and third-harmonic optical response coefficients of ZnSe, ZnTe, and CdTe

Ed Ghahramani

Department of Physics and Ontario Laser and Lightwave Research Centre, University of Toronto, Toronto, Ontario, Canada M5S 1A7

D. J. Moss

National Research Council of Canada, Ottawa, Ontario, Canada K1A 0R6

J. E. Sipe

Department of Physics and Ontario Laser and Lightwave Reserach Centre, University of Toronto, Toronto, Ontario, Canada M5S 1A7

We report full-band-structure calculations of the frequency-dependent second- and third-harmonic response functions of ZnSe, ZnTe, and CdTe, as well as our results for the dielectric function of these semiconductors. We use a linear combination of Gaussian orbitals technique, in conjunction with the $X\alpha$ method, to obtain the energy band structures and optical matrix elements of each material. The expressions for $\overleftrightarrow{\epsilon}(\omega)$ and $\overleftrightarrow{\chi}^{(2)}(-2\omega;\omega,\omega)$ are evaluated utilizing a linearized sampling method for integrating over an irreducible segment of the Brillouin zone; the expression for $\overleftrightarrow{\chi}^{(3)}(-3\omega;\omega,\omega,\omega)$ is evaluated using a random-sampling method. The results of our calculations of $\overleftrightarrow{\epsilon}_2(\omega)$ are in good agreement with experimental results. Our calculated value of $\chi_{14}^{(2)}(0)=24.8\times10^{-8}$ esu for CdTe is in excellent agreement with the measured value [G. H. Sherman and P. D. Coleman, J. Appl. Phys. **44**, 238 (1973)] of $\chi_{14}^{(2)}(\lambda=28\ \mu m)=(28\pm11)\times10^{-8}$ esu. We argue that the experimental results for $\chi_{14}^{(2)}(\lambda=10.6\ \mu m)$ of ZnSe and ZnTe [C. K. N. Patel, Phys. Rev. Lett. **16**, 613 (1966)] are likely to be inaccurate and that there is a need for additional measurements. Our calculations show that both $\overleftrightarrow{\chi}^{(2)}(0)$ and $\overleftrightarrow{\chi}^{(3)}(0)$ are positive for the materials considered in this work. We analyze the prominent features of $\overleftrightarrow{\epsilon}_2(\omega)$, $\overleftrightarrow{\chi}^{(2)}(-2\omega;\omega,\omega)$, and $\overleftrightarrow{\chi}^{(3)}(-3\omega;\omega,\omega,\omega)$ over a wide range of frequencies. Our results indicate that the effects of weak optical transitions are much more pronounced in the second- and third-order optical response functions than in the linear-response functions.

I. INTRODUCTION

The electronic and optical properties of the II-VI semiconductors have been the focus of a number of experimental[1-6] and theoretical[3-5,7-13] investigations over the past three decades. The earlier studies were motivated mainly by a concern with understanding the fundamental physics behind the electronic and optical properties. More recently, possible technological applications of these bulk semiconductors[14-18] and II-VI superlattices[19-25] have provided added impetus for such work.

While there have been numerous full-band-structure calculations of the electronic[3-5,7-13] and linear optical[3-5,9] properties of these semiconductors, to our knowledge there are *no* such studies of the nonlinear optical properties. In fact, in general there are very few full-band-structure calculations of the nonlinear optical properties of semiconductors as a whole. In the past we have carried out full-band-structure calculations of the frequency-dependent second-harmonic generation (SHG) response functions for bulk III-V semiconductors,[26] odd period strained $(Si)_n(Ge)_n/Si$ (001) superlattices,[27] and short period $(GaAs)_m/(AlAs)_n$ superlattices.[28] We have also performed such calculations for the frequency-dependent third-harmonic generation (THG) response

functions for bulk group-IV element and III-V compound semiconductors.[29] Here we report a full-band-structure calculation of the dielectric tensor, $\overleftrightarrow{\epsilon}(\omega)$, and calculations for second- and third-harmonic response functions [$\overleftrightarrow{\chi}^{(2)}(-2\omega;\omega,\omega)$ and $\overleftrightarrow{\chi}^{(3)}(-3\omega;\omega,\omega,\omega)$] of the zinc-blende-structure II-VI semiconductors, ZnSe, ZnTe, and CdTe.

The paper is organized as follows. In Sec. II we give a brief description of the band-structure calculations. We present the formal expressions for the optical response functions in Sec. III. We briefly discuss our numerical integration methods for evaluating these expressions in the same section. In Sec. IV the results of our calculation of $\overleftrightarrow{\epsilon}(\omega)$ are presented and analyzed. Since there have been many analyses of the dielectric function of these semiconductors,[1-6,9] we only briefly describe some of the important features of $\overleftrightarrow{\epsilon}(\omega)$ here, and instead concentrate on the nonlinear properties. We discuss our results for $\overleftrightarrow{\chi}^{(2)}(-2\omega;\omega,\omega)$ in Sec. V. In Sec. VI we present and discuss our results for $\overleftrightarrow{\chi}^{(3)}(-3\omega;\omega,\omega,\omega)$. Finally, our results are summarized in Sec. VII.

II. BAND-STRUCTURE CALCULATIONS

To calculate the energy-band structures and optical matrix elements for ZnSe, ZnTe, and CdTe we use the

minimal basis ($\{1s,2s,2p,3s,3p,3d,4s,4p\}$ orbitals for Zn and Se and $\{1s,2s,2p,3s,3p,3d,4s,4p,4d,5s,5p\}$ orbitals for Cd and Te) linear combination of Gaussian orbitals (MLCGO) technique, in conjunction with the $X\alpha$ method, for constructing the potentials of each material.[11] The local single-site effective potentials and basis functions are constructed by adjusting the α's to produce the correct lowest bulk band gaps. For simplicity we neglect relativistic effects, such as spin-orbit coupling.[11] To ensure convergence we include up to ninth-nearest-neighbor interactions in all of our calculations. Since full details of this approach along with the energy-band struc-

tures for ZnSe, ZnTe, and CdTe have already been discussed by Huang et al.,[11] we shall not present them here. For completeness, we present these band structures along the conventional directions of the fcc Brillouin zone (BZ) in Fig. 1.

III. FORMAL EXPRESSIONS FOR OPTICAL RESPONSE FUNCTIONS

We employ expressions[29] for the optical response coefficients derived within the independent-particle ap-
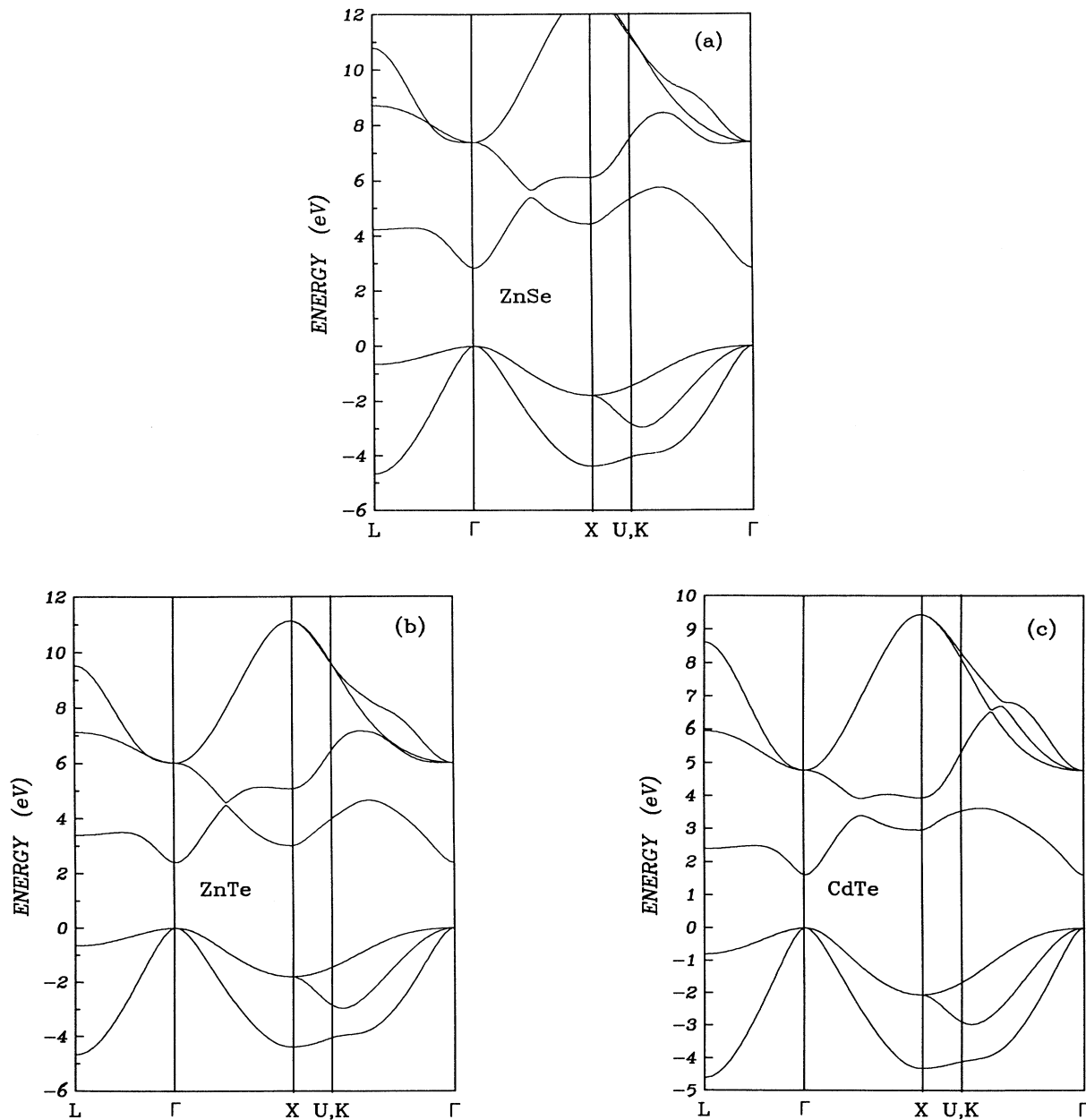
FIG. 1. Energy-band structure of II-VI semiconductors, (a) ZnSe, (b) ZnTe, and (c) CdTe.

proximation, and using the minimal-coupling (MC) interaction Hamiltonian. For simplicity, we neglect local-field corrections. We evaluate the imaginary parts of the response functions first, since they are much simpler because of the presence of the Dirac δ functions. The real parts of the response functions are then obtained from the imaginary parts using Kramers-Kronig relations.[29]

A. Linear optical response

The imaginary part of the dielectric tensor is given by[29]

$$\overleftrightarrow{\epsilon}_2(\omega) = \frac{1}{\pi} \left| \frac{e}{m\omega} \right|^2 \sum_{i,j} \int_{\mathrm{BZ}} f_{ij} \mathbf{p}_{ji} \mathbf{p}_{ij} \delta(E_{ji} - \hbar\omega) d\mathbf{k} , \quad (3.1)$$

where $E = \hbar\omega$, $E_{ji} = E_j - E_i$, $f_{il} = f_i - f_l$, etc., and f_i is the Fermi occupation factor for the single-particle state i. The $\mathbf{p}_{ij}$ are momentum matrix elements. Subscripts i, j, and l can be thought of as labeling the band index at a given $\mathbf{k}$ in the Brillouin zone; quantities like $\mathbf{p}_{ij}$ and E_{jl} are therefore functions of $\mathbf{k}$, which we will often keep implicit. Note that in all of our calculations we ignore the spin-orbit coupling.

To facilitate computation we utilize the cubic symmetry of the zinc-blende semiconductors to convert the integral in (3.1) to one over only an irreducible segment of

the BZ. This is accomplished by applying the operators, P_R, of the group elements R of the symmetry point group (T_d) of these semiconductors to the expansion dyadics $\widehat{i}\,\widehat{j}$ of the dielectric tensor $\overleftrightarrow{\epsilon}(\omega) = \sum_{i,j} \epsilon_{ij} \widehat{i}\,\widehat{j}$. We find

$$\sum_R P_R(\widehat{x}\,\widehat{x}) = \sum_R P_R(\widehat{y}\,\widehat{y}) = \sum_R P_R(\widehat{z}\,\widehat{z}) = 8\overleftrightarrow{\mathbb{1}} ;$$

$$\sum_R P_R(\widehat{i}\,\widehat{j}) = 0, \quad i \neq j , \quad (3.2a)$$

where $\overleftrightarrow{\mathbb{1}}$ is the identity tensor in direct space. Using these symmetry elements and the fact that the BZ has inversion symmetry, the dielectric tensor is given by

$$\overleftrightarrow{\epsilon}_2(\omega) = \frac{16\overleftrightarrow{\mathbb{1}}}{\pi} \left| \frac{e}{m\omega} \right|^2 \sum_{i,j} \int_{\mathrm{IBZ}} f_{ij} |\mathbf{p}_{ij}|^2 \delta(E_{ji} - \hbar\omega) d\mathbf{k} , \quad (3.2b)$$

where IBZ stands for an irreducible segment of the BZ.

B. Second-harmonic generation

The second-harmonic response tensor $\overleftrightarrow{\chi}^{(2)}(-2\omega;\omega,\omega)$ contains contributions from virtual-electron and virtual-hole processes.[27-30] The virtual-electron contribution to the imaginary part of the $\overleftrightarrow{\chi}^{(2)}(-2\omega;\omega,\omega)$ is[29]

$$\overleftrightarrow{\chi}_{ve}''^{(2)}(-2\omega;\omega,\omega) = -\frac{\pi}{2} \left| \frac{e\hbar}{m} \right|^3 \sum_{i,j,l} \int_{\mathrm{BZ}} \frac{d\mathbf{k}}{4\pi^3} \left[\frac{\mathrm{Im}(\mathbf{p}_{jl}^{cc}\mathbf{p}_{li}^{cv}\mathbf{p}_{ij}^{vc})\delta(E_{li} - \hbar\omega)}{E_{li}^3(E_{li} + E_{ji})} - \frac{\mathrm{Im}(\mathbf{p}_{ij}^{vc}\mathbf{p}_{jl}^{cc}\mathbf{p}_{li}^{cv})\delta(E_{li} - \hbar\omega)}{E_{li}^3(2E_{li} - E_{ji})} \right. $$

$$\left. + \frac{16\,\mathrm{Im}(\mathbf{p}_{ij}^{vc}\mathbf{p}_{jl}^{cc}\mathbf{p}_{li}^{cv})\delta(E_{ji} - 2\hbar\omega)}{E_{ji}^3(2E_{li} - E_{ji})} \right] , \quad (3.3)$$

where, e.g., $\mathbf{p}_{ij}^{vc}$ is a momentum-matrix element between a valence state v and conduction state c. Equation (3.3) is not symmetric in the last two Cartesian components; while $\overleftrightarrow{\chi}^{(2)}(-2\omega;\omega,\omega)$ can always be chosen to have this symmetry,[27,29] for cubic materials the use of Eq. (3.5) guarantees this symmetry. The virtual-hole term is similarly given by

$$\overleftrightarrow{\chi}_{vh}''^{(2)}(-2\omega;\omega,\omega) = \frac{\pi}{2} \left| \frac{e\hbar}{m} \right|^3 \sum_{i,j,l} \int_{\mathrm{BZ}} \frac{d\mathbf{k}}{4\pi^4} \left[\frac{\mathrm{Im}(\mathbf{p}_{li}^{vv}\mathbf{p}_{ij}^{vc}\mathbf{p}_{jl}^{cv})\delta(E_{jl} - \hbar\omega)}{E_{jl}^3(E_{jl} + E_{ji})} - \frac{\mathrm{Im}(\mathbf{p}_{ij}^{vc}\mathbf{p}_{jl}^{cv}\mathbf{p}_{li}^{vv})\delta(E_{jl} - \hbar\omega)}{E_{jl}^3(2E_{jl} - E_{ji})} \right. $$

$$\left. + \frac{16\,\mathrm{Im}(\mathbf{p}_{ij}^{vc}\mathbf{p}_{jl}^{cv}\mathbf{p}_{li}^{vv})\delta(E_{ji} - 2\hbar\omega)}{E_{ji}^3(2E_{jl} - E_{ji})} \right] . \quad (3.4)$$

As seen from Eqs. (3.3) and (3.4), resonances can occur when either ω or 2ω is the frequency difference between two single-particle states.

As in the calculation of the linear response, we utilize the crystal symmetry to facilitate the computation. Since

$$\overleftrightarrow{\chi}^{(2)}(-2\omega;\omega,\omega) = \sum_{a,b,c} \chi_{abc}^{(2)}(-2\omega;\omega,\omega)(\widehat{a}\,\widehat{b}\,\widehat{c}) ,$$

we apply the symmetry operators P_R to find

$$\sum_R P_R(\widehat{x}\,\widehat{y}\,\widehat{z})$$

$$= 4(\widehat{x}\,\widehat{y}\,\widehat{z} + \widehat{y}\,\widehat{x}\,\widehat{z} + \widehat{x}\,\widehat{z}\,\widehat{y} + \widehat{y}\,\widehat{z}\,\widehat{x} + \widehat{z}\,\widehat{x}\,\widehat{y} + \widehat{z}\,\widehat{y}\,\widehat{x}) ; \quad (3.5)$$

$$\sum_R P_R(\widehat{a}\,\widehat{b}\,\widehat{c}) = 0 \quad \text{if } a,b,c \text{ not all different} .$$

As seen from Eq. (3.5), for materials with cubic symmetry, $\overleftrightarrow{\chi}^{(2)}(-2\omega;\omega,\omega)$ has only one independent component; we take it to be $\chi_{xyz}^{(2)}(\omega) \equiv \chi_{14}^{(2)}(\omega)$. This component can be evaluated from Eqs. (3.3) and (3.4), utilizing relations (3.5) and the inversion symmetry of the BZ to reduce the integration range to the irreducible segment of the Brillouin zone.

C. Third-harmonic generation

As in the case of $\overleftrightarrow{\chi}^{(2)}(-2\omega;\omega,\omega)$, it is convenient and useful to separate out the different physical contributions

to $\overleftrightarrow{\chi}^{(3)}(-3\omega;\omega,\omega,\omega)$.[29] We find that there are five physically distinct processes contributing to $\overleftrightarrow{\chi}^{(3)}(-3\omega;\omega,\omega,\omega)$:[29] (a) A virtual-electron process, which involves the successive (virtual) excitation of an electron to two conduction bands and then back to the valence band. (b) Three virtual-hole processes. One of these involves the virtual excitation of a conduction-band hole to two successive valence bands and then back to the conduction band. The other two virtual-hole terms involve the successive excitation of both an electron and a hole. (c) A three-state contribution, which may involve the simultaneous (virtual) excitation of two electrons (or holes). In addition, we differentiate between terms that contain diagonal momentum-matrix elements (e.g., $\mathbf{p}_{jj}^{cc}$) and those that do not. Terms containing diagonal-matrix elements we call "intraband;" these vanish in the limit of flat bands. The rest of the terms we label "interband." From Eqs. (3.6) and (3.7), it is clear that the virtual-electron and virtual-hole terms contain intraband contributions, while the three-state term does not. A complete description and a schematic representation of all of the different contributions have been presented earlier.[29]

For a crystal with cubic symmetry the contribution of the virtual-electron processes to the imaginary part of $\overleftrightarrow{\chi}^{(3)}(-3\omega;\omega,\omega,\omega)$ is given by[29]

$$\overleftrightarrow{\chi}_{ve}^{\prime\prime(3)}(-3\omega;\omega,\omega,\omega)$$

$$= -\frac{\pi}{3}\left[\frac{e\hbar}{m}\right]^4 \int_{BZ}\frac{d\mathbf{k}}{4\pi^3}\sum_{i,j,k,l}\mathrm{Re}(\mathbf{p}_{ij}^{vc}\mathbf{p}_{jk}^{cc}\mathbf{p}_{kl}^{cc}\mathbf{p}_{li}^{cv})$$

$$\times\left[\frac{3^6\delta(E_{ji}-3E)}{E_{ji}^4(3E_{ki}-2E_{ji})(3E_{li}-E_{ji})}+\frac{2^7(2E_{ji}-E_{ki})\delta(E_{ki}-2E)}{E_{ki}^4(2E_{li}-E_{ki})(2E_{ji}-3E_{ki})(2E_{ji}+E_{ki})}\right.$$

$$\left.+\frac{\delta(E_{li}-E)}{E_{li}^4(E_{ki}-2E_{li})}\left[\frac{1}{(E_{ji}-3E_{li})}+\frac{2E_{ki}}{(E_{li}+E_{ji})(E_{ki}+2E_{li})}\right]\right]. \tag{3.6}$$

Terms in Eq. (3.6) where $j=k$ or $k=l$ contribute to the intraband response. The contributions of the three virtual-hole terms can be obtained from the virtual-electron term by a set of straightforward substitutions.[29] For the virtual-electron and -hole processes, resonances can occur when either ω, 2ω, or 3ω is the frequency difference between two single-particle states [see Eq. (3.6)].

For a crystal with cubic symmetry, the expression for the three-state contribution to the imaginary part of $\overleftrightarrow{\chi}^{(3)}(-3\omega;\omega,\omega,\omega)$ is given by[29]

$$\overleftrightarrow{\chi}_{\text{three state}}^{\prime\prime(3)}(-3\omega;\omega,\omega,\omega)$$

$$= +\frac{\pi}{3}\left[\frac{e\hbar}{m}\right]^4 \sum_{i,j,k,l}\int_{BZ}\frac{d\mathbf{k}}{4\pi^4}\mathrm{Re}(\mathbf{p}_{ij}^{vc}\mathbf{p}_{jk}^{cv}\mathbf{p}_{kl}^{vc}\mathbf{p}_{li}^{cv})$$

$$\times\left[\frac{3^6\delta(E_{ji}-3E)}{E_{ji}^4(3E_{jk}-E_{ji})(3E_{li}-E_{ji})}\right.$$

$$\left.+\frac{\delta(E_{li}-E)}{E_{li}^4(E_{jk}+3E_{li})}\left[\frac{(E_{lk}+E_{jk})}{(E_{lk}-3E_{li})(E_{ji}+E_{li})}+\frac{(E_{ji}+E_{jk})}{(E_{ji}-3E_{li})(E_{lk}+E_{li})}\right]\right]. \tag{3.7}$$

As seen from Eq. (3.7), for the three-state process resonances can occur only when ω or 3ω is the frequency difference between two single-particle states.

To convert the integration in Eqs. (3.6) and (3.7) to one over only the IBZ, we again use the operations of the symmetry group T_d. Proceeding as in Secs. III A and III B, we find terms such as

$$\sum_R P_R(\hat{x}\,\hat{x}\,\hat{x}\,\hat{x})=8(\hat{x}\,\hat{x}\,\hat{x}\,\hat{x}+\hat{y}\,\hat{y}\,\hat{y}\,\hat{y}+\hat{z}\,\hat{z}\,\hat{z}\,\hat{z}) \tag{3.8}$$

and

$$\sum_R P_R(\hat{x}\,\hat{x}\,\hat{y}\,\hat{y})=4(\hat{x}\,\hat{x}\,\hat{y}\,\hat{y}+\hat{x}\,\hat{x}\,\hat{z}\,\hat{z}+\hat{y}\,\hat{y}\,\hat{x}\,\hat{x}+\hat{y}\,\hat{y}\,\hat{z}\,\hat{z}$$

$$+\hat{z}\,\hat{z}\,\hat{x}\,\hat{x}+\hat{z}\,\hat{z}\,\hat{y}\,\hat{y}). \tag{3.9}$$

An examination of these terms shows[29] that the $\overleftrightarrow{\chi}^{(3)}(-3\omega;\omega,\omega,\omega)$ for a material with cubic symmetry has only two independent components, which we take to be[29] $A\equiv\chi_{1111}^{(3)}(\omega)$ and $B=3\chi_{1212}^{(3)}(\omega)=3\chi_{1221}^{(3)}(\omega)$ $=3\chi_{1122}^{(3)}(\omega)$. Note that, unlike the case of $\overleftrightarrow{\chi}^{(3)}(-2\omega;\omega,\omega)$, $\overleftrightarrow{\chi}^{(3)}(-3\omega;\omega,\omega,\omega)$ must be explicitly symmetrized with respect to the last three Cartesian indices, even for cubic crystals. For cubic materials, this can be accomplished by simply taking (for example)

$$\chi_{1122}^{(3)}(\omega)\equiv\tfrac{1}{3}\{\chi_{1122}^{(3)}(\omega)+\chi_{1212}^{(3)}(\omega)+\chi_{1221}^{(3)}(\omega)\}.$$

These components can be evaluated from Eqs. (3.6) and (3.7), utilizing relations (3.8) and (3.9) and the inversion symmetry of the BZ, to reduce the integration range to the IBZ.

D. Numerical integrations

In this work we use a linearized sampling method[27,28] to evaluate $\epsilon_2(\omega)$ and $\overleftrightarrow{\chi}''^{(2)}(-2\omega;\omega,\omega)$ over the IBZ. This method is very similar to the linear analytic tetrahedra method.[31] The details[27,28] are given elsewhere and will not be repeated here.[27] The expression for $\overleftrightarrow{\chi}''^{(3)}(-3\omega;\omega,\omega,\omega)$ is considerably more complicated than the first- and second-order response functions [Eqs. (3.1) and (3.2)] and (3.6). Therefore, we use a simple random-sampling method to evaluate these functions. This is easier to implement than the linearized methods, but requires substantially more computer time.

In the linearized sampling method we divide the IBM into $15\times15\times15$ cells. Typically these calculations require the use of the equivalent of several hours of Cray Research, Inc. X-MP/22 supercomputer central-processing-unit (CPU) time. The evaluation of $\overleftrightarrow{\chi}''^{(3)}(-3\omega;\omega,\omega,\omega)$, with $\sim 60\,000$ points, is considerably more time consuming. For all calculations, we chose the energy resolution of the bin summation to be 0.02 eV. Although the imaginary parts of the optical response functions do contain resonant-energy denominators [for example, when $2E_{li}=E_{ji}$ in Eq. (3.3)], we do not find any ill-behaved contributions to the response functions for our sampling density. In any case, an examination of the general form of $\overleftrightarrow{\chi}^{(2)}(-2\omega;\omega,\omega)$ and $\overleftrightarrow{\chi}^{(3)}(-3\omega;\omega,\omega,\omega)$ shows that the contributions from such "double resonances" are in fact well behaved.[26,29] The direct evaluation of the real parts of these response functions is more problematic, since the expressions for those terms contain contributions involving resonances in the excitation frequency, rather than just the band energies. Thus, the Kramers-Kronig relations are used to obtain them from the imaginary parts. As a check on the calculations, $\epsilon(0)$, $\overleftrightarrow{\chi}^{(2)}(0)$, and $\overleftrightarrow{\chi}^{(3)}(0)$ were also evaluated directly; the two sets of results typically agreed to better than 5%.

IV. RESULTS FOR LINEAR OPTICAL RESPONSE

Our calculated values of $\overleftrightarrow{\epsilon}_2(\omega)$ for ZnSe, ZnTe, and CdTe, along with the corresponding experimental[6] results, are presented in Fig. 2; we have used a digitizer to extract these experimental values from the plots of Freeouf.[6] As seen from this figure there is good agreement between the theory and experiment. The major discrepancy is due to our neglect of the spin-orbit coupling. In principle we could include this effect in our calculations, but since a full-band-structure evaluation of the nonlinear optical properties is already complex, in the present work we have chosen to ignore it. In any case, we will see below that the nonlinear optical properties— in particular, the $\overleftrightarrow{\chi}^{(3)}(-3\omega;\omega,\omega,\omega)$—are generally dominated by resonances with the E_0 optical peak, where the spin-orbit splitting is not very important.

The important features of $\overleftrightarrow{\epsilon}_2(\omega)$ for ZnSe are as follows. The threshold in $\overleftrightarrow{\epsilon}_2(\omega)$ at 2.84 eV (labeled E_0) is due to the Γ_{15v}-Γ_{1c} transition. The start of the rise around 4.7 eV is due to Λ_{3v}-Λ_{1c} transitions. The major peak at 4.95 eV (labeled E_1) is caused by L_{3v}-L_{1c} transitions. Note that in the experimental measurements this

peak is split in two by spin-orbit coupling. The small bulge at around 6.3 eV (labeled E_2') is caused by Δ_{5v}-Δ_{1c} transitions. The slight shoulder at around 6.6 eV (labeled E_2'') is due to Σ_{2v}-Σ_{1c} transitions. Finally, the last major peak at 6.82 eV (labeled E_2) is due to a sum of Δ_{5v}-Δ_{1c} and Σ_{2v}-Σ_{1c} transitions. The major features of $\overleftrightarrow{\epsilon}_2(\omega)$ for ZnTe and CdTe are similar to that of ZnSe.
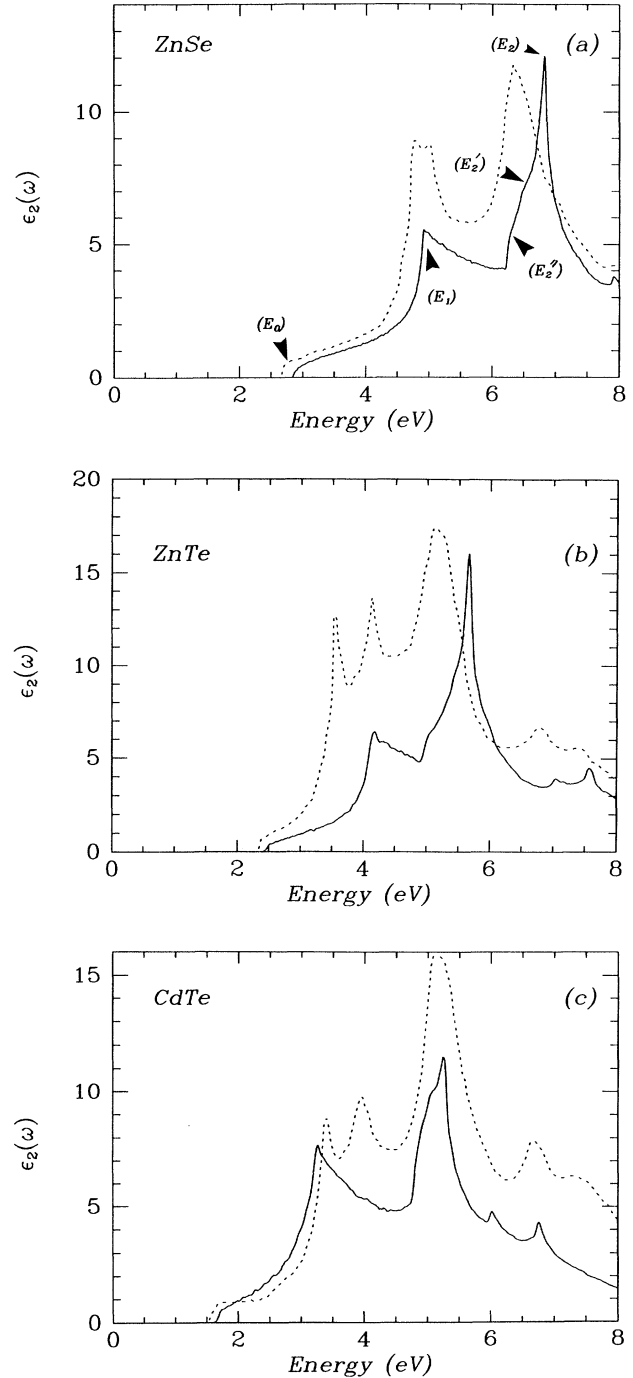
FIG. 2. Results for $\overleftrightarrow{\epsilon}_2(\omega)$ for II-VI semiconductors, (a) ZnSe, (b) ZnTe, and (c) CdTe. The experimental results (dotted line) are from Ref. 6.

V. SECOND-HARMONIC GENERATION

Our results for the imaginary and real part of the $\overleftrightarrow{\chi}^{(2)}(-2\omega;\omega,\omega)$ are presented in Figs. 3 and 4, respectively. In our calculation we have included both the virtual-electron and virtual-hole contributions, although as in the case of the III-V semiconductors the latter is much smaller than the former[26,30] (see Table I).
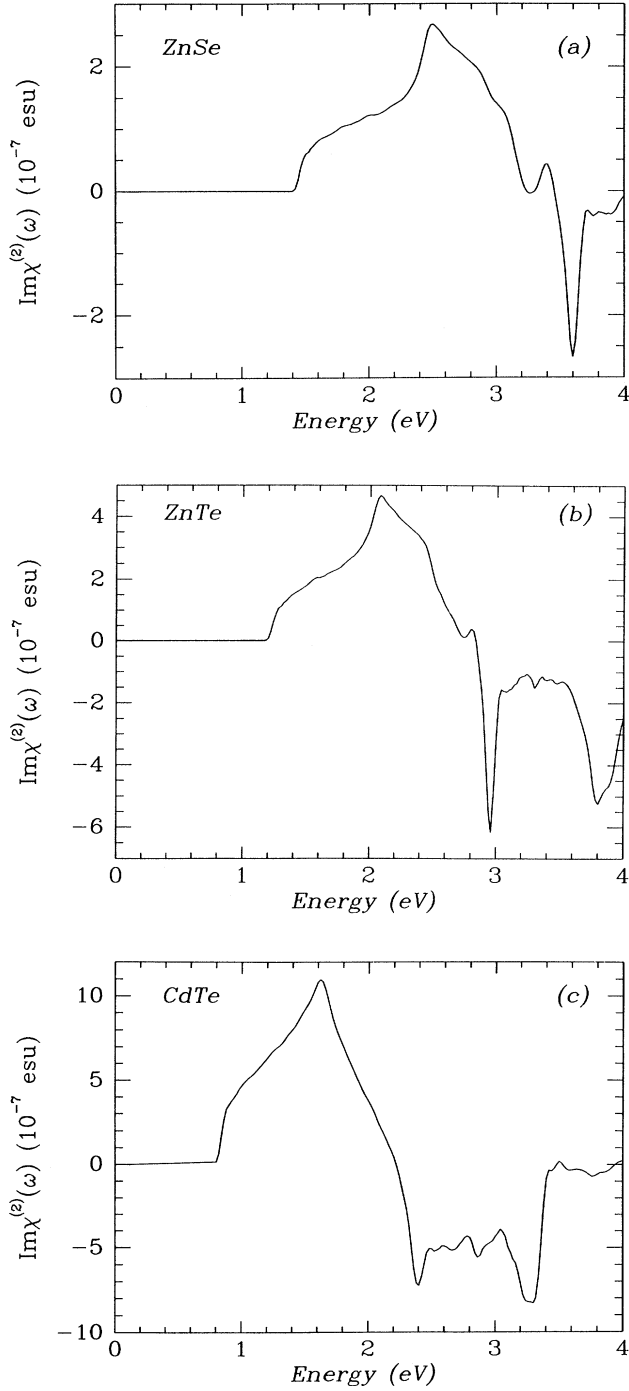
FIG. 3. Results for the imaginary part of $\overleftrightarrow{\chi}^{(2)}(-2\omega;\omega,\omega)$ for II-VI semiconductors, (a) ZnSe, (b) ZnTe, and (c) CdTe.
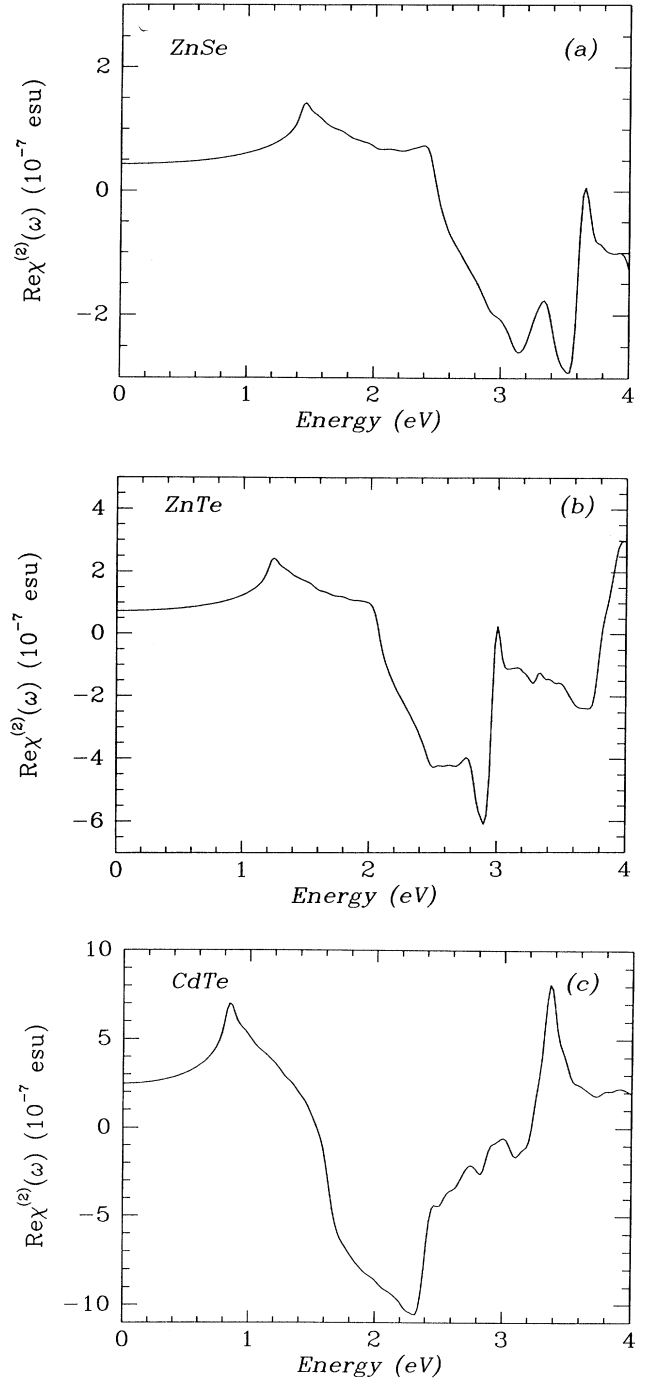
FIG. 4. Results for the real part of $\overleftrightarrow{\chi}^{(2)}(-2\omega;\omega,\omega)$ for II-VI semiconductors, (a) ZnSe, (b) ZnTe, and (c) CdTe.

TABLE I. Theoretical results for $\chi_{12}^{(2)}(0)$ of II-VI semiconductors in units of 10^{-8} esu.

	ZnSe	ZnTe	CdTe
Virtual electron	4.2	6.9	24.3
Virtual hole	0.2	0.4	0.5
Total	4.4	7.3	24.8

Our calculated values of $\chi_{14}^{(2)}(0)$ for ZnSe, ZnTe, and CdTe are presented in Table I. Note that $\chi_{14}^{(2)}(0)$ for all the semiconductors considered here is positive. Based on a simplified band model for $\overline{\chi}^{(2)}(-2\omega;\omega,\omega)$, Aspnes[30] has shown that the sign of $\overline{\chi}^{(2)}(0)$ depends on the choice of the coordinate system for the positions of the anion and cation in the unit cell. For example, if the coordinate system is chosen such that the cation (say Zn) and anion (say Se) are located at $(0,0,0)$ and $(a/4)(1,1,1)$, respectively, where a is the lattice constant, then one expects $\overline{\chi}^{(2)}(0) > 0$. This is indeed in agreement with the results of our full-band-structure calculations. This fact has also been experimentally verified by Miller and Nordland.[32]

From Table II it is clear that there is significant discrepancy between the experimental results of $\chi_{14}^{(2)}$ for ZnSe, ZnTe, and CdTe. Sherman and Coleman[34] (SC) have discussed this discrepancy in some detail. First of all, SC point out that the earlier results of Patel[35] were obtained in the early days of CO_2-laser technology and, due to certain technical difficulties, the resulting unknown beam profile makes accuracy doubtful.[34] SC (Ref. 34) also performed a simple model calculation of $\overline{\chi}^{(2)}(-2\omega;\omega,\omega)$ for CdTe in order to show that the factor of ~ 3 enhancement in $\chi_{14}^{(2)}$ at $\lambda = 10.6$ μm as measured by Patel,[35] over their value measured at $\lambda = 28.0$ μm, could not be accounted for by the contribution of optical-phonon resonances. They[34] pointed out that not only was their result at $\lambda = 28.0$ μm in good agreement with results of this model calculation, but also that it agreed quite well with independent experimental data for the electro-optic coefficient.[36]

We would like to point out that the two sets of existing experimental measurements, Patel[35] and Soref and Moos,[37] (SM) are not consistent with each other. Patel's result for $\chi_{14}^{(2)}$ for SHG in ZnSe, at $\lambda = 10.6$ μm, is actually *larger* than SM's result at $\lambda = 1.06$ μm. Since $\lambda = 1.06$ μm lies slightly lower than half of the band gap,[38] $\chi_{14}^{(2)}$ for SHG at this wavelength should be considerably larger than at $\lambda = 10.6$ μm. Also, Patel's measurement in ZnTe is not that much smaller than SM's result; since $\lambda = 1.06$ μm is almost exactly half of the band gap,[38] one would expect $\chi_{14}^{(2)}$ for SHG at $\lambda = 1.06$ μm to be significantly larger than at $\lambda = 10.6$ μm. Finally, while our result of $\chi_{14}^{(2)} = 24.8 \times 10^{-8}$ esu for CdTe is in excellent agreement with SC's (Ref. 34) measured value of $(28 \pm 11) \times 10^{-8}$ esu, it is in considerable disagreement with Patel's[35] results.

TABLE II. Experimental results for $\chi_{14}^{(2)}$ of II-VI semiconductors in units of 10^{-8} esu. Note that $\chi_{14}^{(2)} = 2d_{14}$, where d_{14} is the second-harmonic coefficient (Ref. 33).

Experiment	λ (μm)	ZnSe	ZnTe	CdTe
SC[a]	28			28±11
Patel[b]	10.6	37±14	44±16	80±30
SM[c,d]	1.06	22	73	

[a]Reference 34.
[b]Reference 35.
[c]References 30 and 33.
[d]Reference 37.

For these reasons, together with other remarks made by SC,[34] we might expect the results for $\chi_{14}^{(2)}(0)$ of ZnSe and ZnTe to be roughly a factor of 3 lower than the values reported by Patel (the same factor by which the results of SC for $\chi_{14}^{(2)}(0)$ in CdTe differ from that of Patel[35]). Such lower values, if indeed experimentally verified, would considerably improve the agreement between theory and experiment. Based on the same arguments, we are inclined to expect that the experimental results of SM,[37] which were obtained even earlier than those of Patel,[35] are also not accurate. To our knowledge there are no measurements of $\chi_{14}^{(2)}$ for ZnSe and ZnTe other than those of Patel[35] and SM.[37] Therefore, we propose that further measurements of $\chi_{14}^{(2)}$ for these two materials should be undertaken to clarify these discrepancies.

In order to give an idea of the size of the $\overline{\chi}^{(2)}(0)$ in these semiconductors relative to other materials, in Table III we present the results of our full-band-structure calculations of $\chi_{14}^{(2)}(0)$ for AlP, AlAs, GaAs, GaSb, and InSb (III-V compound semiconductors).[39] Interesting patterns arise when the results of Tables I and II are compared. First, by comparing semiconductors which have the same last valence shell numbers (i.e., ZnSe and GaAs, ZnTe and GaSb, and CdTe and InSb) we see that the values of $\overline{\chi}^{(2)}(0)$ for the II-VI materials are much smaller than those of their III-V counterparts. Furthermore, the values of $\overline{\chi}^{(2)}(0)$ for ZnSe, ZnTe, and CdTe are comparable to those of the III-V materials with one less valence shell (AlP, AlAs, and GaAs, respectively). From a band-structure point of view this pattern can simply be understood as follows. The energy denominators involved in the expressions for $\overline{\chi}^{(2)}(-2\omega;\omega,\omega)$ are of the form $E_{conduction} - E_{valence}$ or $E_{conduction} - E_{conduction}$. In II-VI semiconductors, the conduction bands and the energy differences between them lie at much higher energies than in III-V materials. Therefore, the denominators of $\overline{\chi}^{(2)}(-2\omega;\omega,\omega)$ for II-VI materials are generally larger than those of the III-V materials, which in turn results in smaller second-order response functions.

The results of our calculations for the magnitude of $\overline{\chi}^{(2)}(-2\omega;\omega,\omega)$ are presented in Fig. 5. The prominent features of the SHG response functions of ZnSe are as follows. The first peak is mainly due to a 2ω resonance with the E_0 optical peak. Because of the strong $(\sim E^{-5})$ energy dependence of $\overline{\chi}^{(2)}(-2\omega;\omega,\omega)$, this peak is almost comparable in size to the other major peaks. This is in contrast to the size of the E_0 peak in $\overline{\epsilon}(\omega)$ (energy dependence $\sim E^{-3}$) where it is much smaller than the size of the other peaks. The third peak is due to the ω resonance with the E_1 optical peak. The fourth peak is due to a 2ω resonance with the E_2' optical peak. The dip around 3.3 eV is due to interference between 2ω resonances with the E_2'' and E_2 optical peaks. The important features of

TABLE III. Theoretical results for $\chi_{14}^{(2)}(0)$ of III-V semiconductors in units of 10^{-8} esu, obtained using LCGO in conjunction with the $X\alpha$ method, as in this paper.

AlP	AlAs	GaAs	GaSb	InSb
4.7	7.2	24.9	82.2	360.0

ZnTe and CdTe are similar to that of ZnSe. Note that contributions of the resonance with the E_2' and E_2'' optical peaks to SHG are much more pronounced than the corresponding contributions to $\bar{\epsilon}_2(\omega)$.
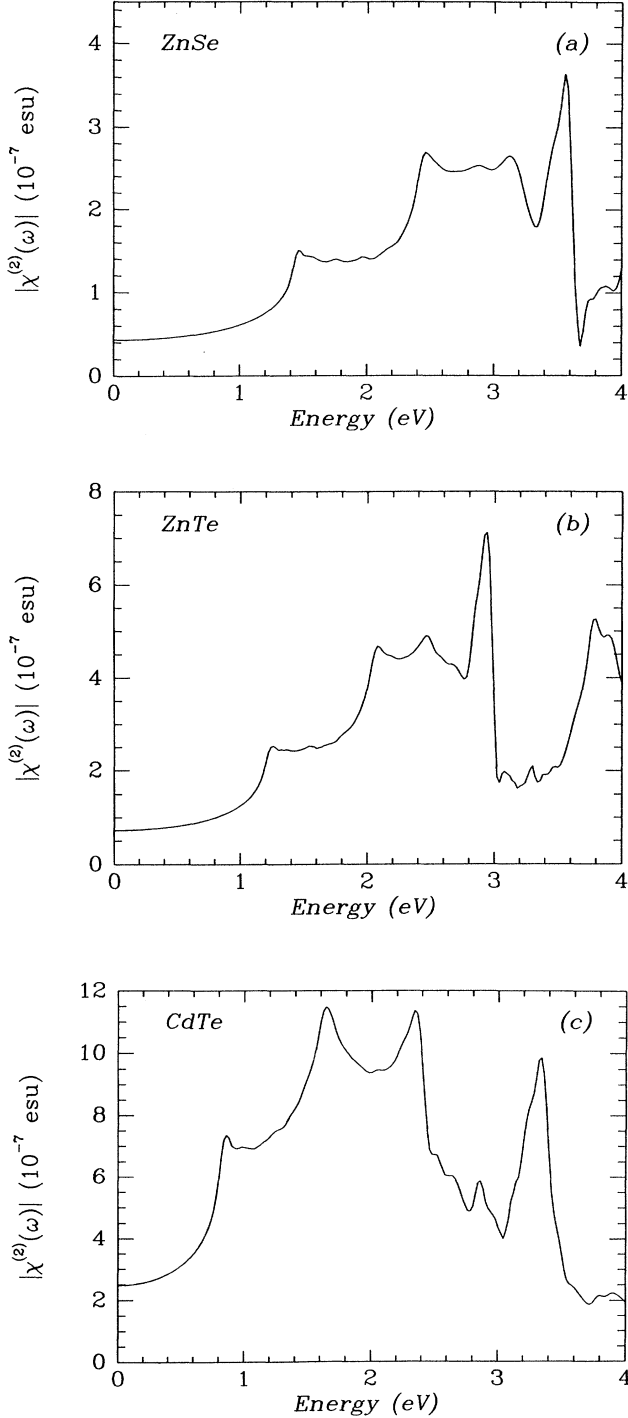
FIG. 5. Results for $|\bar{\chi}^{(2)}(-2\omega;\omega,\omega)|$ for II-VI semiconductors, (a) ZnSe, (b) ZnTe, and (c) CdTe.

TABLE IV. Theoretical results for $\chi_{1111}^{(3)}(0)$ in units of 10^{-12} esu. The virtual-electron and virtual-hole results only include the interband response, while the intraband result includes all contributions from both virtual-electron and virtual-hole terms.

	ZnSe	ZnTe	CdTe
Virtual electron	−1.2	−2.8	−12.4
Virtual hole	−1.6	−3.1	−10.8
Intraband	−2.8	−5.7	−21.1
Three state	5.8	12.2	44.6
Total	0.2	0.6	0.3

VI. THIRD-HARMONIC GENERATION

A. Zero-frequency limit of $\bar{\chi}^{(3)}(-3\omega;\omega,\omega,\omega)$

Our results for different contributions to $\bar{\chi}^{(3)}(0)$ for all three materials are presented in Tables IV and V. In all cases only the three-state term is positive, and dominates all of the other terms, including the intraband term. This can be understood in terms of a simple model as follows. The expression for $\bar{\chi}^{(3)}(0)$ obtained using the MC interaction Hamiltonian is the same for either a localized two-level single-particle system, or a solid (with a minimal sp^3 basis set) whose electrons are very tightly bound (referred to as a solid in the tight-binding limit[29]), and is given by[29,40]

$$\bar{\chi}^{(3)}(0) = +\frac{1}{3}\left[\frac{e\hbar}{m}\right]^4 |\mathbf{p}_{10}|^4 \frac{1}{E_g^7}$$
$$\times [(3^5+1)+3(3^3+1)+3^2(3+1)] , \quad (6.1)$$

where $\mathbf{p}_{10}$ is the momentum-matrix element between two localized single-particle states of the system $|0\rangle$ and $|1\rangle$ and $E_g = E_1 - E_0$ is the difference between the energies of the two levels. This corresponds to the three-state term, and it is clear that it is always *positive*. Now for a solid, when the tight-binding condition is relaxed, one might expect $\bar{\chi}^{(3)}(0)$ to still be dominated by the (positive) three-state term.[29] As seen from Table III, in fact, $\bar{\chi}^{(3)}(0)$ is positive for these semiconductors.

As expected, the size of the $\bar{\chi}^{(3)}(-3\omega;\omega,\omega,\omega)$ of the heavier elements is in general larger than that of the lighter elements, since the former have smaller band gaps than the latter. The only exception to this rule is $\chi_{1111}^{(3)}$

TABLE V. Theoretical results for $3\chi_{1212}^{(3)}(0)$ in units of 10^{-12} esu. The virtual-electron and virtual-hole results only include the interband response, while the intraband result includes all contributions from both virtual-electron and virtual-hole terms.

	ZnSe	ZnTe	CdTe
Virtual electron	−1.2	−3.0	−15.2
Virtual hole	−1.9	−3.7	−13.3
Intraband	−5.4	−11.5	−42.4
Three state	9.6	20.4	77.6
Total	1.1	2.2	6.7

for CdTe, which at very low frequencies is smaller than the corresponding response of ZnTe. We are unable to give an explanation for this anomalous behavior.

We would like to point out that to our knowledge there are no experimental measurements of $\overleftrightarrow{\chi}^{(3)}(-3\omega;\omega,\omega,\omega)$ at any frequency for the materials considered here. It would be interesting to see how well experimental measurements agree with our calculated results.

B. Dispersion in $\overleftrightarrow{\chi}^{(3)}(-3\omega;\omega,\omega,\omega)$

We present our results for the imaginary and real parts of $\overleftrightarrow{\chi}^{(3)}(-3\omega;\omega,\omega,\omega)$ in Figs. 6 and 7, respectively. The results of our calculations for the magnitude of $\overleftrightarrow{\chi}^{(3)}(-3\omega;\omega,\omega,\omega)$ are shown in Fig. 8. The prominent features of the third-harmonic response function of ZnSe are as follows. The first peak is mainly due to a 3ω reso-
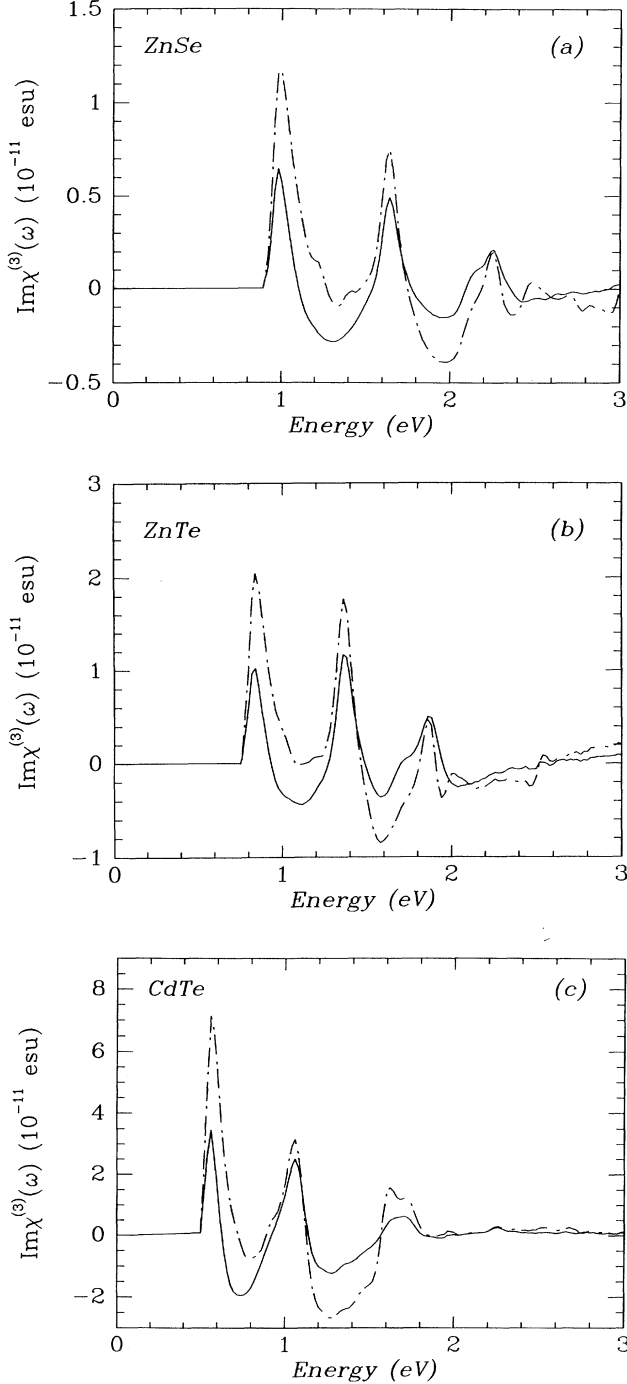
FIG. 6. Results for the imaginary part of $|\chi^{(3)}_{1111}(\omega)|$ (solid line) and $\chi^{(3)}_{1212}(\omega)$ (dashed-dotted line) for II-VI semiconductors, (a) ZnSe, (b) ZnTe, and (c) CdTe.
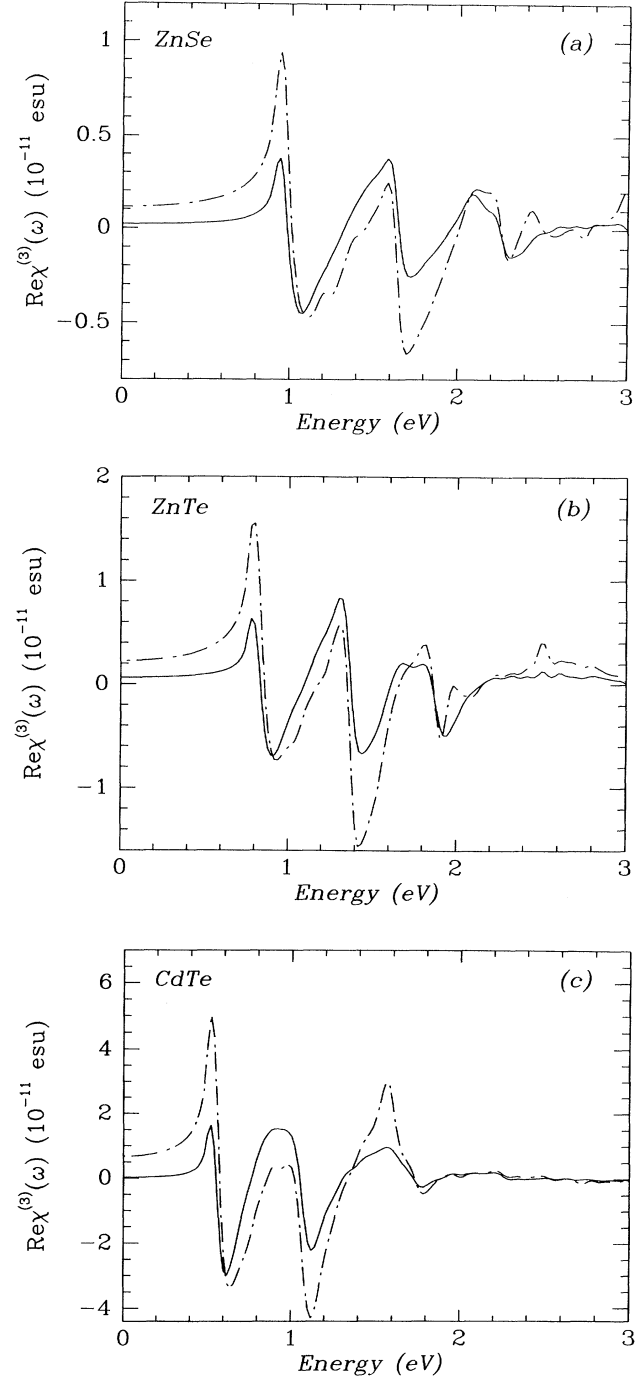
FIG. 7. Results for the real part of $|\chi^{(3)}_{1111}(\omega)|$ (solid line) and $\chi^{(3)}_{1212}(\omega)$ (dashed-dotted line) for II-VI semiconductors, (a) ZnSe, (b) ZnTe, and (c) CdTe.
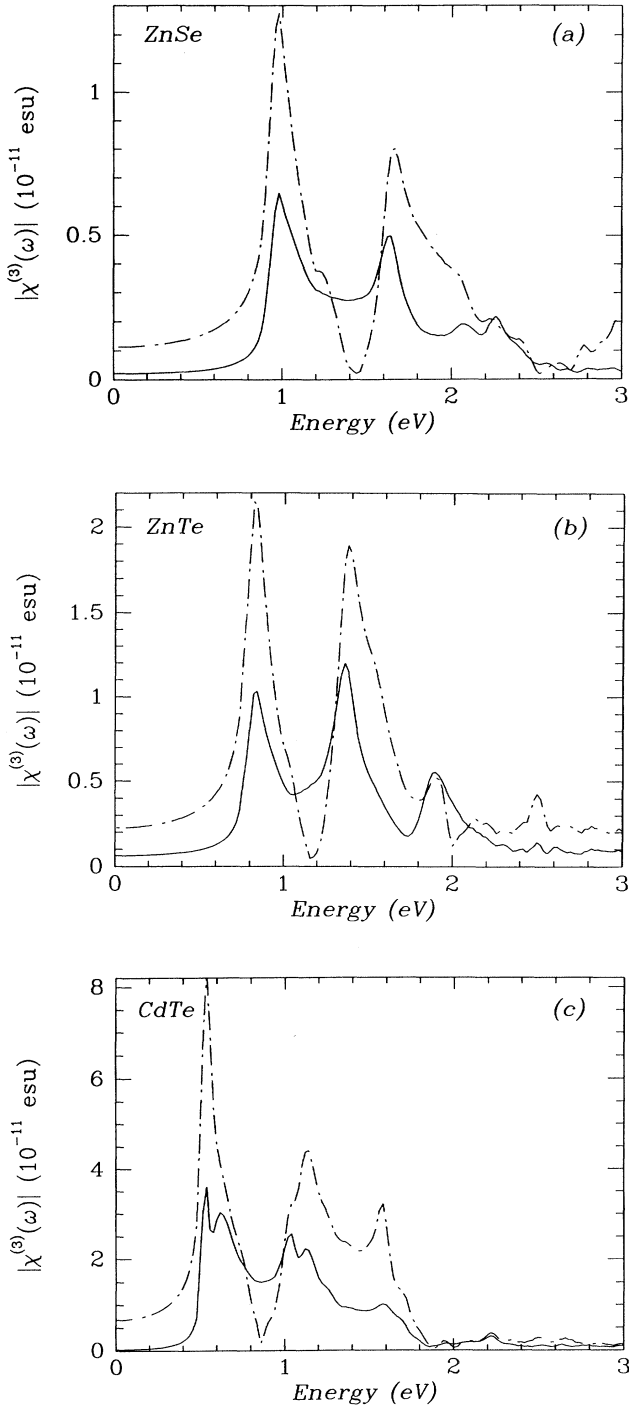
FIG. 8. Results for $|\chi^{(3)}_{1111}(\omega)|$ (solid line) and $|\chi^{(3)}_{1212}(\omega)|$ (dashed-dotted line) for II-VI semiconductors, (a) ZnSe, (b) ZnTe, and (c) CdTe.

nance with the E_0 optical peak. Due to the strong ($\sim E^{-7}$) energy dependence of $\overleftrightarrow{\chi}^{(3)}(-3\omega;\omega,\omega,\omega)$,[29] its structure will be dominated by the 3ω resonance with the E_0 critical point in materials where the lowest conduction band at the Brillouin-zone center is nondegenerate, such as those considered here.[29] Therefore, we expect

the other peaks to be smaller in size than the first. The second peak for the most part is the result of destructive interference between a 2ω resonance with the E_0 optical peak and a 3ω resonance with the E_1 optical peak. As seen from Eq. (3.7) the three-state term, which is dominant, has no 2ω contributions; the 2ω resonance with the E_0 optical peak is due to the other terms. On the other hand, the 3ω resonance with the E_1 optical peak is mainly due to the three-state term. Furthermore, the two contributions have different signs: the three-state term gives positive contributions, and other terms negative contributions. Finally, the third and fourth peaks are due to interferences of 3ω resonances with E_2', E_2'', and E_2 optical peaks. The important features of ZnTe and CdTe can be similarly identified.

VII. CONCLUSIONS

We have performed the full-band-structure calculation of the frequency-dependent second- and third-harmonic response functions in ZnSe, ZnTe, and CdTe. We have also carried out full-band-structure calculations of the dielectric function of these materials. The calculations were performed with the minimal coupling, or **p· A**, interaction Hamiltonian, using standard perturbation theory and neglecting local-field corrections. The results of our calculations of $\overleftrightarrow{\epsilon}_2(\omega)$ are in good agreement with experimental results. Our calculated value of $\overleftrightarrow{\chi}^{(2)}(0)=24.8\times10^{-8}$ esu for CdTe is in excellent agreement with the measured value[34] of $\overleftrightarrow{\chi}^{(2)}(0)=(28\pm11)\times10^{-8}$ esu. We have argued that the experimental results of Patel[35] and Soref and Moos[37] are likely to be inaccurate and that there is a need for additional measurements.

We have analyzed the prominent features of $\overleftrightarrow{\epsilon}_2(\omega)$, $\overleftrightarrow{\chi}^{(2)}(-2\omega;\omega,\omega)$, and $\overleftrightarrow{\chi}^{(3)}(-3\omega;\omega,\omega,\omega)$ over a wide range of frequencies. Our results indicated that the effects of weak optical transitions are much more pronounced in second- and third-order optical response functions than in the linear-response functions. We find that the sign of $\overleftrightarrow{\chi}^{(2)}(0)$ and $\overleftrightarrow{\chi}^{(3)}(0)$ is positive for all elements considered here, and that $\overleftrightarrow{\chi}^{(3)}(0)$ is dominated by the interband response. The nonlinear-response functions of the II-VI materials are much smaller than those of the III-V materials. Furthermore, the values of $\overleftrightarrow{\chi}^{(2)}(0)$ of ZnSe, ZnTe, and CdTe are comparable to those of the III-V materials with one less valence shell, i.e., AlP, AlAs, and GaAs, respectively.

[1]M. Cardona and G. Harbeke, Phys. Rev. **137**, 1467 (1965).

[2]M. Cardona, M. Welnstein, and G. A. Wolff, Phys. Rev. **140**, 633 (1965).

[3]Y. Petroff, M. Balkanski, J. P. Walter, and M. L. Cohen, Solid State Commun. **7**, 549 (1969).

[4]J. P. Walter, M. L. Cohen, Y. Petroff, and M. Balkanski, Phys. Rev. B **1**, 2661 (1970).

[5]D. J. Chadi, J. P. Walter, and M. L. Cohen, Phys. Rev. B **5**, 3058 (1972).

[6]J. L. Freeouf, Phys. Rev. B **7**, 3810 (1973).

[7]J. R. Chelikowsky and M. L. Cohen, Phys. Rev. B **14**, 556 (1976).

[8]A. Zunger and A. J. Freeman, Phys. Rev. B **17**, 4850 (1978).

[9]C. S. Wang and B. M. Klein, Phys. Rev. B **24**, 3393 (1981); **24**, 3417 (1981).

[10]K. J. Chang, S. Froyen, and M. L. Cohen, Phys. Rev. B **28**, 4736 (1983).

[11]M. Z. Huang and W. Y. Ching, J. Phys. Chem. Solids **46**, 977 (1985).

[12]J. E. Bernard and A. Zunger, Phys. Rev. B **36**, 3199 (1987).

[13]A. Continenza, S. Massidda, and A. J. Freeman, Phys. Rev. B **38**, 12 996 (1988).

[14]Q. Fu, A. V. Nurmikko, L. A. Kolodziejski, R. L. Gunshor, and J. W. Wu, Appl. Phys. Lett. **51**, 578 (1987).

[15]S. K. Chang, D. Lee, H. Nakata, A. V. Nurmikko, L. A. Kolodziejski, and R. L. Gunshor, J. Appl. Phys. **62**, 4835 (1987).

[16]O. Ohkawa, T. Mitsuyu, and O. Yamazaki, J. Appl. Phys. **62**, 3216 (1987).

[17]T. Yasuda, I. Mitsuichi, and H. Kukimoto, Appl. Phys. Lett. **52**, 57 (1988).

[18]H. Cheng, J. M. Depuydt, J. E. Potts, and T. L. Smith, Appl. Phys. Lett. **52**, 147 (1988).

[19]J. N. Schulman and T. C. McGill, J. Vac. Sci. Technol. **16**, 1513 (1979).

[20]Y. Rajakarunanayake, R. H. Miles, G. Y. Wu, and T. C. McGill, Phys. Rev. B **37**, 10 212 (1988).

[21]C. G. Van de Walle, K. Shahzad, and D. Olego, J. Vac. Sci. Technol. B **6**, 1350 (1988).

[22]A. Imai, M. Kobayashi, S. Dosho, M. Kongai, and K. Takahashi, J. Appl. Phys. **64**, 647 (1988).

[23]H. Yang, A. Ishida, and H. Fujiyasu, J. Appl. Phys. **65**, 2838 (1989).

[24]Y. H. Wu, H. Yang, A. Ishida, and H. Fujiyasu, Appl. Phys. Lett. **54**, 239 (1989).

[25]H. Yang, A. Ishida, and H. Fujiyasu, Appl. Phys. Lett. **56**, 2114 (1990).

[26]D. J. Moss, J. E. Sipe, and H. M. van Driel, Phys. Rev. B **36**, 9708 (1987).

[27]E. Ghahramani, D. J. Moss, and J. E. Sipe, Phys. Rev. Lett. **64**, 2815 (1990); Phys. Rev. B **43**, 8990 (1991).

[28]E. Ghahramani, D. J. Moss, and J. E. Sipe, Phys. Rev. B **43**, 9269 (1991).

[29]D. J. Moss, E. Ghahramani, J. E. Sipe, and H. M. van Driel, Phys. Rev. B **41**, 1542 (1990).

[30]D. E. Aspnes, Phys. Rev. B **6**, 4648 (1972).

[31]D. J. Moss, J. E. Sipe, and H. M. van Driel, Phys. Rev. B **36**, 1153 (1987), and references cited therein.

[32]R. C. Miller and W. A. Nordland, Phys. Rev. B **2**, 4896 (1970); **5**, 4931 (1972).

[33]D. A. Kleinman, Phys. Rev. B **2**, 3139 (1970).

[34]G. H. Sherman and P. D. Coleman, J. Appl. Phys. **44**, 238 (1973).

[35]C. K. N. Patel, Phys. Rev. Lett. **16**, 613 (1966).

[36]For references see Fig. 2 of Ref. 34.

[37]R. A. Soref and H. W. Moos, J. Appl. Phys. **35**, 2152 (1964).

[38]For the values of band gaps, see Ref. 11.

[39]Edwin Ghahramani, Ph.D. thesis, University of Toronto, 1990 (unpublished).

[40]David J. Moss, Ph.D. thesis, University of Toronto, 1988 (unpublished).